Flow-induced shear stress and deformation of a core-shell structured microcapsule in a microchannel

Tuo Hou[1, 2], Yong Ren[1,2,3*], Yue Chan[4], Jing Wang[5,6], Yuying Yan[7]

[1]Research Group for Fluids and Thermal Engineering, University of Nottingham Ningbo China, Ningbo, China
[2]Department of Mechanical, Materials and Manufacturing Engineering, University of Nottingham Ningbo China, Ningbo, China
[3]Key Laboratory of Carbonaceous Wastes Processing and Process Intensification Research of Zhejiang Province, University of Nottingham Ningbo China, Ningbo, China
[4]Institute for Advanced Study, Shenzhen University, Shenzhen, China
[5]Department of Electrical and Electronic Engineering, University of Nottingham Ningbo China, Ningbo, China
[6]Key Laboratory of More Electric Aircraft Technology of Zhejiang Province, University of Nottingham Ningbo China, Ningbo, China
[7]Faculty of Engineering, University of Nottingham, University Park, Nottingham NG7 2RD, UK

[*]Email: yong.ren@nottingham.edu.cn

Abstract

A numerical model was developed and validated to investigate the fluid-structure interactions between fully developed pipe flow and core-shell structured microcapsule in a microchannel. Different flow rates and microcapsule shell thicknesses were considered. A 6th order rotational symmetric distribution of von Mises stress over the microcapsule shell can be observed on the microcapsule with a thinner shell configuration, especially at higher flow rate conditions. It is also observed that when being carried along in a fully developed pipe flow, the microcapsule with a thinner shell tends to accumulate stress at a higher rate compared to that with a thicker shell. In general, for the same microcapsule configuration, higher flow velocity would induce a higher stress level over the microcapsule shell. The deformation gradient was used to capture the microcapsule's deformation in the present study. The effect of Young's Modulus on the microcapsule shell on the microcapsule deformation was investigated as well. Our findings will shed light on the understanding of the stability of core-shell structured microcapsule when

subjected to flow-induced shear stress in a microfluidic system, enabling a more exquisite control over the breakup dynamics of drug-loaded microcapsule for biomedical applications.

Keywords: microfluidics, double emulsion, microcapsule, fluid-structure interaction

1 Introduction

The microcapsules are micro-objects with core-shell structures and characteristic sizes of 1-1000 microns. The intrinsic structure enables the encapsulation of dispersed solid, gaseous, or liquid substances in the inner core which can be separated by the solid outer shell as a barrier from the external environment, thus degradation of active substances will be avoided. Therefore microcapsules have been widely used as vehicles to deliver functional materials including drugs, chemical reactants, gases, and enzymes in a plethora of applications such as food and beverages, cosmetics, biochemical sensors, drug delivery, and chemical catalyst reactions [1-2]. The conventional microcapsule fabrication methods such as interfacial polymerization [3], polymer phase separation [4], and electrospray [5] normally result in the formation of microcapsules with polydispersed size distribution and thus highly variable load levels and poor control over the release characteristics. The droplet microfluidic technology has attracted growing attention in recent years [6]. The microfluidic channels with different flow configurations such as hydrodynamic focusing, coaxial flow, T-shaped channels, and step flow channels can generate emulsion droplets with high size monodispersity [7]. The precise control over the size, structure, and shape of the droplets with good repeatability can be achieved by adjusting the geometric dimensions and flow conditions of the microchannels [8-11]. The double emulsion can be formed using different flow channels such as co-flow and focusing microcapillary device, double cross-junction channel, T-junction combined with cross junction channel, double T-junction channel,

and double bifurcation channel. The double emulsion formation process involves the use of three immiscible liquids which interact in the microchannel to overcome the interfacial tension and induce the interface instability so that the inner phase liquid is divided into dispersed liquid beads, which are embedded in the middle phase, which are surrounded by the continuous outer phase to generate double emulsions such as water/oil/water[12], oil/water/oil[13], water/water/water[14]. Different materials such as polydimethylsiloxane (PDMS), polyethylene glycol diacrylate and N-isopropyl acrylamide, hexanediol diacrylate, and tripropylene glycol diacrylate can be used in the middle phase. With the aid of photopolymerization [15], self-assembly [16], phase change [17], cross-linking [18], nanoparticle adsorption on the water/oil interface [19] or nanoparticle adsorption on the liquid/gas interface [20], the double emulsion droplets can be applied as a template to fabricate microcapsules or microcolloids with a core-shell structure in various applications [21-28]. In drug delivery systems, the drug administration route has an important impact on the delivery of the drug in the organisms and directly affects the drug release kinetics. The common routes of administration include arterial injection, intravenous injection, subcutaneous and intramuscular injection, as well as the gastrointestinal and digestive tract. The conventional drug administration routes have poor targeting efficacy, requiring oral administration or injections multiple times. The drug delivery by microcapsules can significantly prolong the activity of the drug, and control the release rate of the drug in a tunable manner, thus can help to reduce the number of medications and improve the patients' compliance. The hydrophilic drugs are usually loaded in the hydrogel microcapsules made by alginate or chitosan, and hydrophobic drugs are usually loaded in the polymer microcapsules made by polylactic acid and polylactic acid-polyglycolic acid copolymer [29]. There are three main ways to release the encapsulated substances from microcapsules: membrane rupture, diffusion, and degradation of the capsule

membrane. Membrane rupture is the destruction of the microcapsule shell due to extrusion and friction, and the core material is released as the shell material dissolves; the diffusion is mainly achieved by the selection of an appropriate shell material that has a penetrating effect, and the core material gradually dissolves and diffuses outwards until the concentration inside and outside the capsule reaches an equilibrium; degradation of the microcapsule refers to the destruction of the capsule and release of the enclosed substances by the influence of heat, solvents, enzymes, or microorganisms. The passive drug release characteristics are affected by the microcapsule size, monodispersity, cross-linking method, and the porosity of the shell. The external stimulus such as pH change [30], chemical reactions [31], temperature change [32], or external stress [33] can also control the release kinetics of microencapsulated drugs actively.

Despite the latest advances in applying microfluidic emulsification technology to generate microcapsules for drug delivery, and other biomedical applications [34], there are still some problems that have not been adequately studied or fully understood, and more comprehensive, systematic, and in-depth analyses are needed.

(1) Fluid-structure coupling is a common multiphysics phenomenon, in which fluid flow will deform the solid structure, and the latter will further change the fluid flow boundary conditions. The interaction between fluid and structure is ubiquitous in many natural phenomena and engineering systems. Several studies have been conducted on the flow of microcapsules in a microfluidic channel in recent years [35-40], and the adhesion of microcapsules with different sizes and shapes on the blood vessels has also been reported [41]. The flow of viscous fluid in contact with the solid shell of the microcapsules will exert stress on the solid-liquid interface. The stress field of the viscous fluid is affected by the dynamic change of the structure, and the stress

field can affect the mechanical properties of the microcapsules, which in turn affects the release kinetics of the microcapsules.

(2) Soft polymers such as PDMS have excellent optical transparency, gas permeability, and biocompatibility, which are essential for cell culture on biochips and are widely used in cell engineering and medicine, biological tissue engineering, and other fields. PDMS can be used as a microcapsule shell in lab-on-a-chip systems to study drug delivery in blood vessels [42]. The deformation of a thin PDMS shell can affect fluid flow and cause pressure drop changes [43]. However, the complex fluid-solid coupling effect produced by this flexible material has not been studied adequately.

(3) It is very difficult to experimentally measure the flow field of compound droplets in a microdevice, this is not only because the invasive methods will interfere with the flow conditions in the microchannel, but also because the particle image velocimetry (PIV), particle tracking velocimetry (PTV) and laser-induced fluorescence (LIF) technologies normally have an optical distortion at the interface. Alternatively, computational fluid dynamics (CFD) has shown its potential in analyzing complex flow fields surrounding the double emulsion in the microchannel.

Herein, a numerical model has been developed to investigate the effect of flow conditions such as inlet flow rate, and the microcapsule properties such as the shell thickness and Young's Modulus on the deformation of microcapsules flowing in a microchannel. The work will shed light on an in-depth understanding of the fluid-structure interaction phenomenon in microsystems for drug delivery applications.

2. Numerical Model

A 2D numerical model was developed to investigate the fluid-structural interaction between the flow inside of a straight microchannel and a core-shell structured microcapsule of various shell thicknesses at various inflow velocities.

2.1 Governing Equations, Geometry, and Meshing

The basic equations governing the fluid motion are mass and momentum conservation:

$$\frac{\partial \rho}{\partial t} + \nabla \cdot (p\vec{v}) = 0$$

$$\frac{\partial}{\partial t}(\rho\vec{v}) + \nabla(\rho\vec{v}\vec{v}) = -\nabla \mathrm{p} + \nabla \cdot (\bar{\bar{\tau}}) + \vec{F}$$

Where ρ stands for the density of the fluid, p is the static pressure, $\bar{\bar{\tau}}$ is the stress tensor, and $\vec{F}$ represents the external body forces (for instance from the interaction with the solid structure), respectively.

At the current setup, the microchannel is considered as a straight rigid-walled tube, with an inner diameter of 1 mm and a length of 14 mm. An illustrative figure is shown below to indicate the dimensions of the current geometry setup. The microcapsule is core-shell structured, with a liquid core of water and a solid shell of polydimethylsiloxane (PDMS). The fluid carrying the microcapsule inside the microchannel is also set to be water. The microcapsule in this work has an outer diameter of 0.25 mm, with various shell thicknesses.

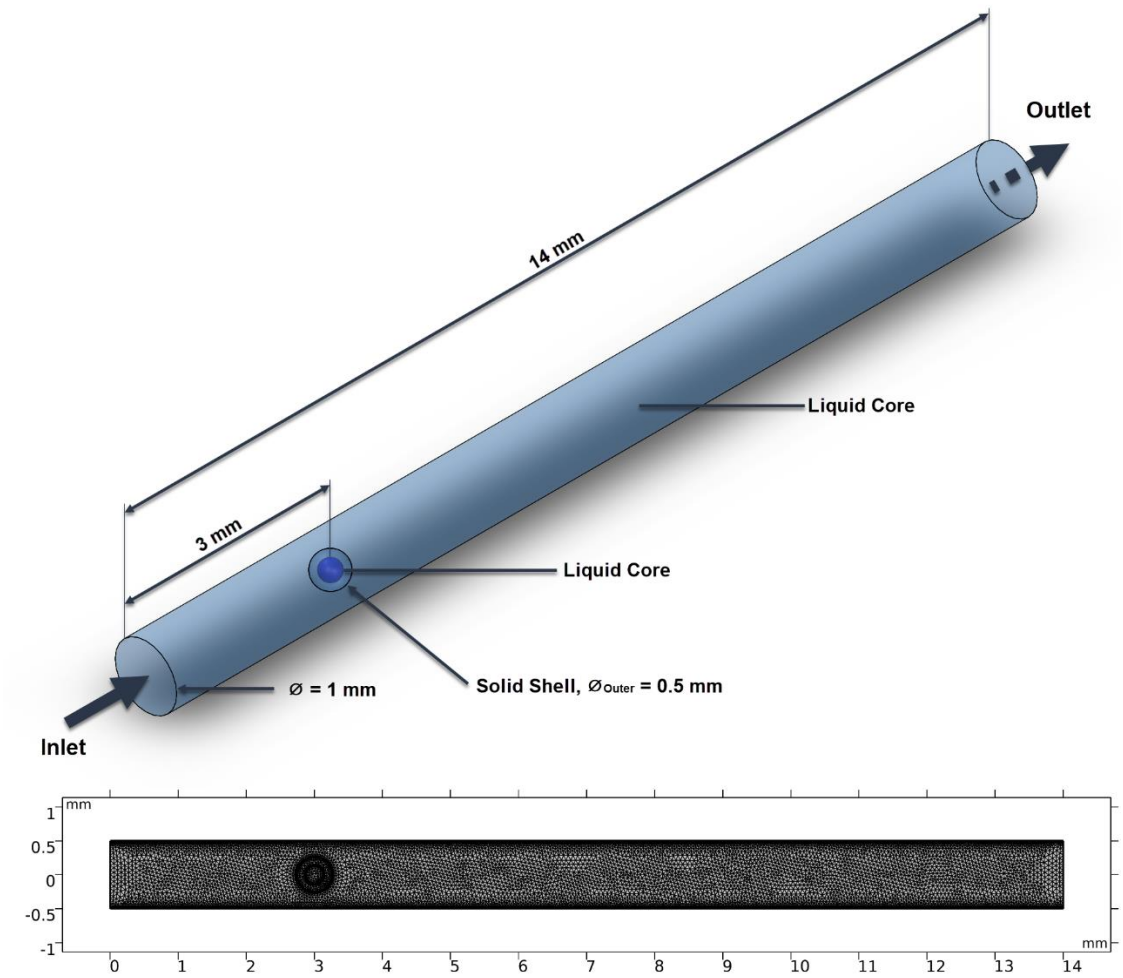

Figure 1 Schematic of the microchannel geometry and the meshing of the 2D model setup with the microcapsule (shell thickness: 0.1 mm), located at the initial position

During the simulation, various inlet flow velocity was applied, the most aggressive of which being 0.2 m/s, in which case the Reynolds number of this configuration can be calculated as:

$$Re = \frac{\rho V L}{\mu} = \frac{998.29 kg/m^3 \times 0.2 m/s \times 1 mm}{1.002 \times 10^{-3} N \cdot s/m^3} \approx 200$$

Where ρ and μ stand for the density and the dynamic viscosity of water, accordingly. V stands for the flow velocity of the flow and L represents the characteristic length, in this case, being the diameter of the microchannel. For the current work, the inlet flow velocity ranges from 0.05 m/s to 0.2 m/s, thus

the flow inside the microchannel for this work can be considered laminar under every working condition.

To produce consistent results, it is essential to make sure the flow inside of the microchannel is fully developed at the initial position of the microcapsule. For the current laminar pipe flow, an empirical formula to determine the entrance length is available from Bergman et al. [44], and considering the most aggressive condition:

$$Ln = 0.06Re \cdot D = 1.94mm$$

Thus, as indicated in Figure 1, the initial position of the microcapsule center being set to 3 mm downstream of the inlet should be appropriate for this study.

The mesh was generated using the predefined meshing tool within the Comsol software, with the normal mesh size preset. To be more specific, the maximum element size is 0.938 mm and the minimum is 0.0042 mm. The maximum element growth rate is 1.3, and the curvature factor is 0.3. Special treatments were applied to solid-liquid interfaces. The mesh for a typical setup of this study is shown in Figure 1.

A mesh sensitivity study was conducted to double-check that the mesh size of choice is suitable for this work and partially served as a validation for the numerical framework established. Four different preset mesh configurations for the Comsol software were chosen, to capture a radial direction flow velocity profile at 7 mm downstream of the entrance of the previously proposed microchannel, and the flow velocity was set to be 0.15 m/s. It can be observed that the flow is fully developed at the chosen location. Legends in Figure 2A indicate different predefined meshing options in Comsol, where the “Coarser” option yields a mesh with a maximum element size of 0.087 mm; “Coarse”, 0.067 mm; “Normal”, 0.045 mm; “Fine”, 0.028 mm, accordingly. An analytical solution for fully developed laminar pipe flow from White et al. [47] was also plotted

as a reference. From Figure 2A, apart from the coarser meshing preset in Comsol, good matches can be found between the analytical solution and numerical solutions using the current model. Although the Coarse meshing preset has shown a good capability of capturing the fluid information, to more precisely look into the FSI phenomenon between the fluid and the microcapsule, and also allow more space for moving mesh, the Normal meshing preset was adopted in the actual study.

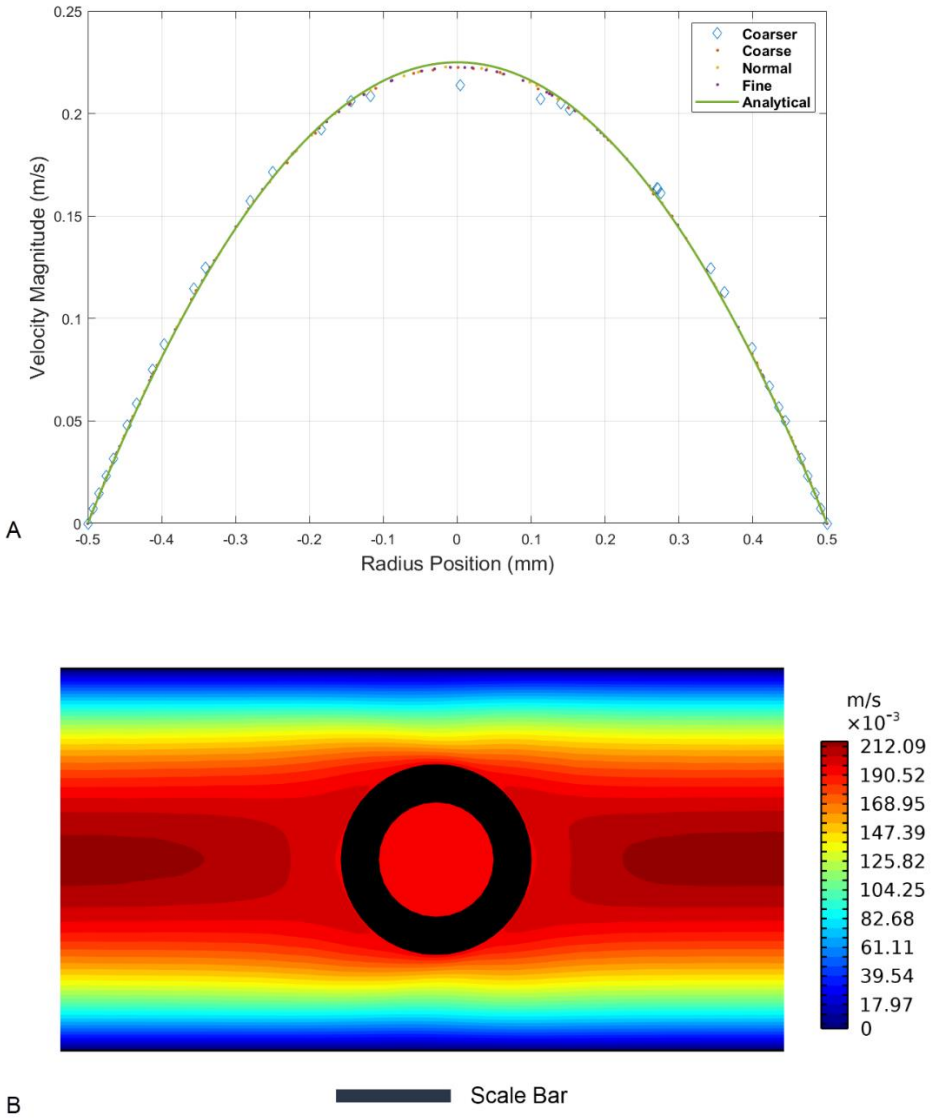

Figure 2 A: Radial direction flow velocity profile at 0.7 mm downstream of the inlet for various mesh configurations. Flow velocity = 0.15 m/s. Legends indicate different predefined meshing options in Comsol, where the "Coarser" option yields a mesh with a maximum element size of 0.087 mm; "Coarse", 0.067 mm; "Normal", 0.045 mm; "Fine", 0.028 mm, accordingly; B: Contour of velocity magnitude in the vicinity of the microcapsule. Inflow velocity: 0.15 m/s, δ^* = 0.4, time = 0.02 s; Scale bar represents 0.2 mm

To account for the microcapsule's influence on the flow inside of the microchannel, the velocity magnitude of the flow near the microcapsule was investigated with our numerical framework, at conditions of inflow velocity = 0.15 m/s, with the microcapsule of shell thickness of $\delta^* = 0.4$. The plot was captured at time = 0.02 s after release. It can be observed from Figure 2B that the presence of the microcapsule greatly altered the in-duct flow profile, and the velocity magnitude distribution difference between the upstream side (left side) and the downstream side (right side) shows that the microcapsule is been carried by the moving flow.

Also, it seems that at our current setting for contour precision (30 levels), no obvious internal circulation is observed, and the internal flow velocity seems to be uniform. This might be attributed to the physical blockage effect due to the presence of the solid microcapsule shell such that the flow in the vicinity of the microcapsule will not give rise to the perturbation of the flow inside the microcapsule.

It is also of importance to investigate how an off-centered initial release of the microcapsule would influence the flow and the movement of the microcapsule in the microchannel. The microcapsule with the same $\delta^* = 0.4$ has been released at different positions with various y-direction offset at the flow velocity of 0.15 m/s. All plots are captured at 0.02 s after the release of the microcapsule, and this is consistent with that in Figure 2B when there is no offset.

2.2 Materials, Numerical Methods, and A Brief Validation

The fluid in this study, as well as the inner liquid core of the microcapsules, are both set to be liquid water, and the shell material of the microcapsules are set to be polydimethylsiloxane (PDMS). For the proposed FSI investigation of this work, the Comsol software was utilized to

conduct the numerical simulation. The default material properties were adopted during the study and a table of parameters of materials used in this work is shown in Table 1.

Table 1 Material properties

Fluid	Water	Density	$998.29\ kg/m^3$
		Viscosity	$1.002 \times 10^{-3}\ N \cdot s/m^3$
Solid	PDMS	Density	$970\ kg/m^3$
		Young's modulus	$750\ kPa$
		Poisson's Ratio	0.49

The Solid material was assumed to be linear elastic. This work considers the mechanical properties of polydimethylsiloxane (PDMS), and the density, Young's modulus, and Poisson's ratio adopted in this work are 970 kg/m3, 750 kPa, and 0.49, respectively. The Bond number of the capsule in the current setup was calculated as:

$$Bo = \frac{\Delta\rho g l^2}{\sigma} \approx 0.00001 \ll 1$$

Where g stands for the gravitational acceleration, l stands for the characteristic length of the capsule (diameter), $\Delta\rho$ stands for the density difference between the PDMS and liquid water, and σ for the surface tension of the capsule. The gravity effect of the microcapsule is thus neglected.

A Fluid-Structure Interaction study was conducted using the abovementioned mode based on the finite element method within Comsol. The quadratic Lagrange method was used to describe the displacement field of the solid part (microcapsule shell). As for the fluid discretization, both the

velocity components and the pressure field were discretized using 1st order elements for the sake of the flow's laminar nature and the numerical robustness. FSI couplings appear on the boundaries between the fluid and the solid. The Comsol Fluid-Structure Interaction interface uses an arbitrary Lagrangian-Eulerian (ALE) method to combine the fluid flow formulated using an Eulerian description and a spatial frame with solid mechanics formulated using a Lagrangian description and a material (reference) frame. The fluid and structure were fully coupled in this work. A time-dependent study was conducted using the abovementioned model, with a time range of 0 to 0.2 s, and a time step of 0.002 s. The implicit backward differentiation formula (BDF) was used for time-stepping methods in the time-dependent solver which uses backward differentiation formulas with variable discretization order (maximum of 2nd order by our setting) and automatic step-size selection. To improve the convergence performance of our model, the initial time step was set to be 0.001 s.

In the present study, four different inlet flow velocity conditions were considered, namely 0.05 m/s, 0.1 m/s, 0.15 m/s and 0.2 m/s. According to an analytical solution for fully developed laminar pipe flow from White et al. [46]:

$$u_{max} = \left(-\frac{dp}{dx}\right)\frac{R^2}{4\mu}$$

where for a fully developed laminar pipe flow, the u_{max} equals to twice the unified inlet velocity, and R stands for the radius of the flow field and μ for the viscosity of the fluid; $\frac{dp}{dx}$ indicates how static pressure of the flow field changes along the axial direction. From the outlet zero-gauge pressure boundary condition and an inflow velocity of 0.2 m/s, it can be calculated that the static pressure inside the channel near the middle section of the channel is

$$p_0 = 3.2\ Pa.$$

An equation for the calculation of the Hoop stress for a thin shell sphere proposed by Ozturk, Y. et al. [48] was adopted for the current configuration:

$$\sigma_H = \frac{p_0 r}{2t} \approx 4$$

which corresponds to a von Mises stress of the same amount. The numerical result for the above condition is on the same scale as the above-calculated outcome, the current numerical framework is thus considered validated.

To validate the deformation response with the results reported in existing literature, a succinct parallel plate compression simulation was carried out based on our proposed numerical framework. Good matches were found with experimental results provided by Do Nascimento et al. [49] and a more detailed description of the validation method can be found in the supplementary material.

3. Results and Discussion

In the current study, various shell thicknesses and flow velocities were considered, to investigate how different shell thicknesses and flow conditions would affect the load on the microcapsule imposed by the fluid.

As found in existing literature, such as the work by Mercadé-Prieto et al. [45], von-Mises stress can be used as an effective indicator for the load applied on such core-shell structured microcapsules. Higher the load on the microcapsule leads to higher von-Mises stress on the microcapsule shell, thus the microcapsule is more likely to break. As for the case studied in this work, the load and von-Mises stress are very small compared to the amount required for capsule rupture, yet the von-Mises stress can still be considered a useful tool to indicate the load on the

microcapsule. Thus the von Mises Stress on the microcapsule shell was analyzed within the Comsol software.

According to COMSOL's official documents, the von-Mises Stresses are computed using axial stress, bending axial stress, bending shear stresses, and torsional shear stresses. The axial stress is computed as:

$$\sigma_N = \frac{N}{A}$$

Where N is the axial force. The bending axial stresses are computed around the first principal axis (σ_{M1}) and around the second principal axis (σ_{M2}). The bending shear stresses are computed with 2 sets of components of shear stresses. The components of the first shear stress caused by a shear force T_1 along the x1 axis are τ_{T1x} and τ_{T1y}. Similarly, the components of the shear stress caused by a shear force T_2 along the x2 axis are τ_{T2x} and τ_{T2y}. In both cases, the resultants are computed as: $\tau_{T1} = \sqrt{\tau_{T1x}^2 + \tau_{T1y}^2}$ and $\tau_{T2} = \sqrt{\tau_{T2x}^2 + \tau_{T2y}^2}$. The components of the shear stress caused by Saint-Venant torsion are:

$$\tau_{Mtx} = \frac{M_t \phi_{,y}}{J}$$

$$\tau_{Mty} = \frac{M_t \phi_{,x}}{J}$$

Where M_t is the twisting moment. The resultant is computed as: $\tau_{Mt} = \sqrt{\tau_{Mtx}^2 + \tau_{Mty}^2}$, and the von-Mises equivalent stress is computed from the stress components defined above:

$$\sigma_{vM} = \sqrt{(\sigma_N + \sigma_{M1} + \sigma_{M2})^2 + 3(\tau_{T1x} + \tau_{T2x} + \tau_{Mtx})^2 + 3\left(\tau_{T1y} + \tau_{T2y} + \tau_{Mty}\right)^2}$$

For the current study involves FSI between the fluid and the microcapsule, and the microcapsule would be carried along by the moving fluid from the abovementioned initial position, we shall allow a few time steps for the microcapsule to accelerate to achieve a stable condition in the flow. For better convergence performance, the Backward Euler method for consistent initialization was applied for the time-dependent solver and may introduce additional numerical errors for initial time steps [46], which provides another motive for neglecting results from initial time steps.

3.1 von Mises Stress Distributions over the Microcapsule Shell

The surface average von Mises stress can be calculated for each configuration at every flow velocity for every time frame. When looking into the generated surface average von Mises stress for each configuration, an oscillation pattern can be observed for each case. The oscillation pattern tends to narrow down to a certain value, which is considered the stable average surface von Mises stress for one configuration, and this oscillation pattern can be used as an indicator for determining whether the microcapsule has been stable in the flow. It can also be observed that for the same flow velocity, the microcapsule with a thicker shell tends to take longer to achieve stable conditions. The time history of the surface average von Mises stress of each configuration showing this pattern is attached as appendix data.

To describe the microcapsule shell thickness more conveniently, a dimensionless microcapsule shell thickness was adopted in this study:

$$\delta^* = \frac{\delta}{R}$$

Where δ is the microcapsule shell thickness, and R is the radius of the microcapsule. The resulting δ^*would be the dimensionless shell thickness. The microcapsule modeled in the current study share an outer radius (0.25 mm), with 3 different shell thickness adopted, namely 0.05 mm,

0.1 mm, and 0.15 mm, corresponding to the dimensionless capsule shell thickness of: $\delta^* = 0.2$, $\delta^* = 0.4$, $\delta^* = 0.6$, respectively.

Images of the von Mises stress distribution over various microcapsule shells of different thicknesses at various velocities are shown in Figure 3. In each subplot, the chosen time frame is different, which is based on the abovementioned method to make sure the microcapsule has achieved a stable condition when capturing its stress distribution. Sub figures in Figure 3 shows the plots of flow velocity at 0.05 m/s, 0.1 m/s, 0.15 m/s and 0.2 m/s, from A to L, accordingly. For all configurations, symmetrical distribution can be found along the flow direction. Moreover, a rotational symmetric distribution of von Mises stress over the microcapsule shell can also be observed on dimensionless capsule shell thickness of $\delta^* = 0.2$ and $\delta^* = 0.4$ configurations, especially at higher flow velocities.

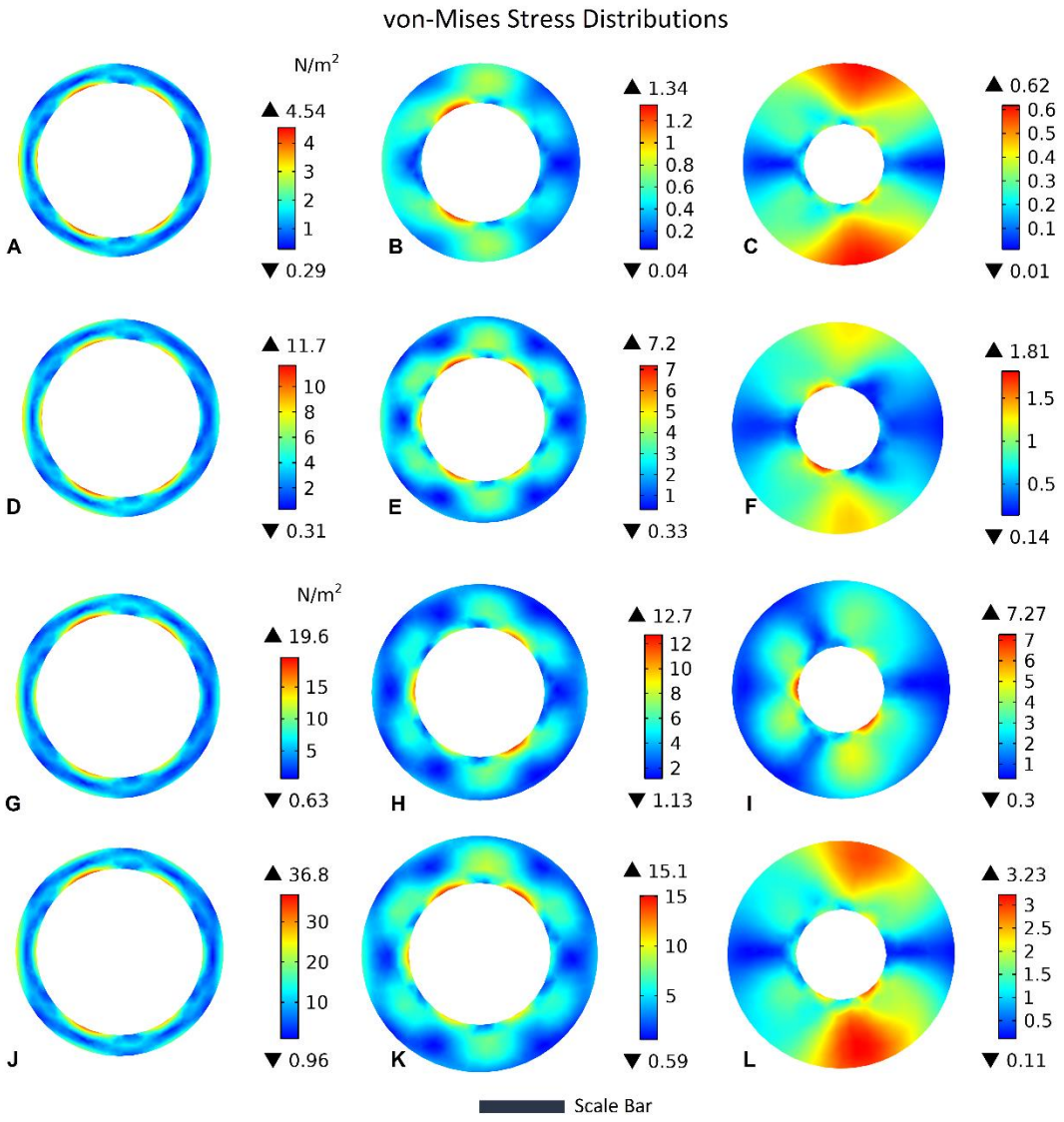

Figure 3 Images of von Mises stress distribution over microcapsule shells of different thicknesses at a flow velocity of 0.05 m/s (A-C), 0.1 m/s (D-F), 0.15 m/s, (G-I), and 0.2 m/s (J-L), the dimensionless shell thickness from left to right are δ^*=0.2, δ^*=0.4, and δ^*=0.6, accordingly. The scale bar represents 0.2 mm

As for the $\delta^* = 0.2$ microcapsule, a rotational symmetry distribution of order 6 can be observed at all flow velocities, yet for the $\delta^* = 0.4$ microcapsule, the 6^{th} order rotational symmetry in stress distribution can only be observed at higher flow velocities, and such rotational symmetry doesn't

exist at all for the $\delta^* = 0.6$ microcapsule. The above 6^{th} order rotational symmetry observed shows that, for certain configurations, the stress concentration can happen at multiple positions along with the capsule shell. This may provide some novel insights on the breaking up mechanism of such core-shell structured microcapsules. From the above results, a general trend can be observed, that a higher flow velocity would induce a higher shell von Mises stress level over the microcapsule shell, and so would a thinner shell thickness. This trend would be discussed in more detail within the following section.

3.2 Surface Average von Mises Stress over the Microcapsule Shell

As mentioned in section 3.1, a method based on the oscillation pattern in microcapsule shell average von Mises stress that tends to narrow down to near a certain value was proposed as a tool to determine whether the microcapsule that is being carried along by the moving fluid has achieved a (relatively) stable condition. The mean stable von Mises stresses over each configuration can be acquired by averaging the surface average von Mises stress over a period where the capsule has achieved its stable condition.

As for the calculated averaged mean surface average von Mises stress, all three configurations have shown a tendency of increasing their stress level when exposed to a higher flow velocity. It can be seen in Figure 4A, that the $\delta^* = 0.2$ microcapsule is most sensitive to flow velocity changes. The $\delta^* = 0.4$ and the $\delta^* = 0.6$ microcapsules have shown relatively similar responses to the change of flow velocity, yet the overall trend can be described as When being carried along in a fully developed pipe flow, the microcapsule with a thinner shell tends to accumulate stress at a higher rate compared to that with a thicker shell.

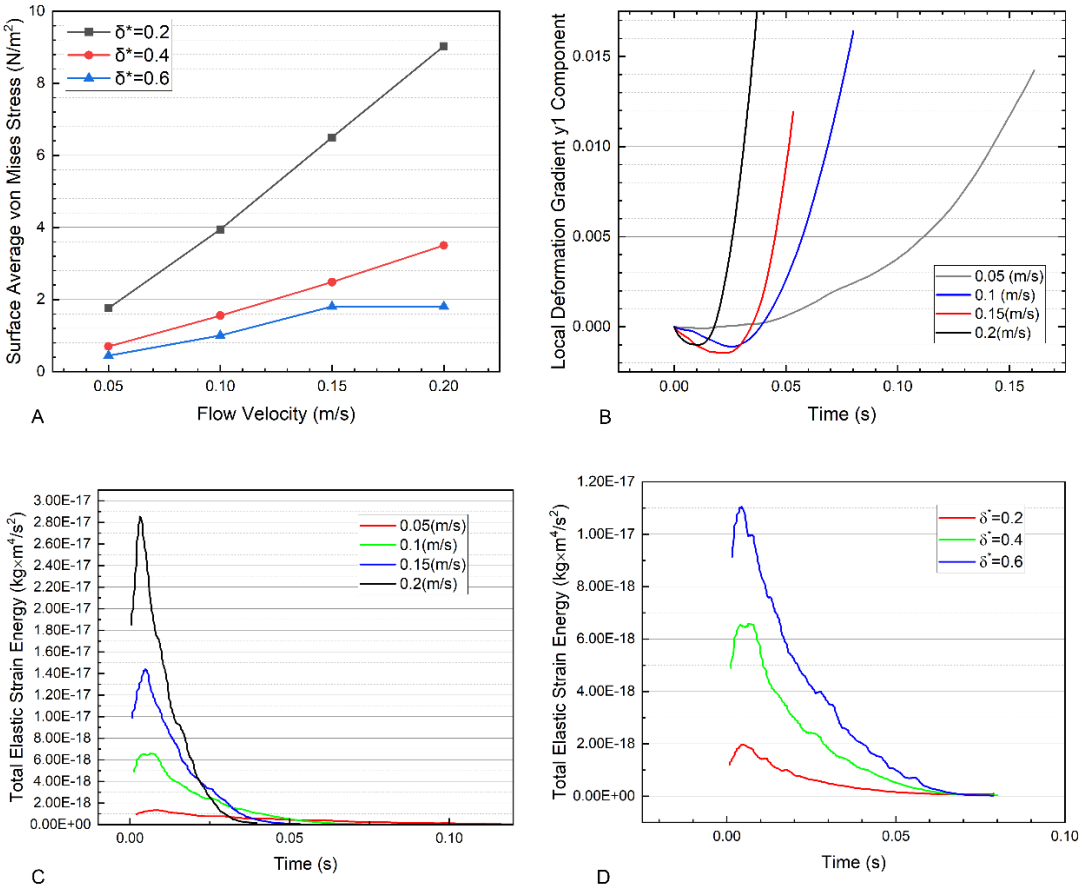

Figure 4 A: Microcapsule Shell Surface Average von Mises Stress trends in terms of different capsule shell thickness and flow velocity; B: The local deformation gradient y1 component of the microcapsule of δ*=0.4 under various flow velocities; C: The integrated elastic strain energy over the δ*=0.4 capsule under different flow velocities; D: The integrated elastic strain energy for different shell thickness under the same 0.1m/s flow velocity

3.3 Investigation of Microcapsules' Deformation

The deformation gradient contains the full information about the local rotation and deformation of the material and is thus considered a great tool to describe the deformation response of the microcapsules in the current study. The deformation gradient **F** is defined as:

$$\boldsymbol{F} = \frac{\partial \boldsymbol{x}}{\partial \boldsymbol{X}} = \boldsymbol{I} + \frac{\partial \boldsymbol{u}}{\partial \boldsymbol{X}}$$

where the coordinates **X** denote the original location of the material particle, and the coordinates $\boldsymbol{x} = \boldsymbol{x}(\boldsymbol{X},\ t)$ denote the new location where the material particle has been moved to after a certain time t. For the current 2D setup, the above definition can be shown in matrix form:

$$\boldsymbol{F} = \begin{bmatrix} \frac{\partial x}{\partial X} & \frac{\partial x}{\partial Y} \\ \frac{\partial y}{\partial X} & \frac{\partial y}{\partial Y} \end{bmatrix} = \begin{bmatrix} 1 + \frac{\partial u}{\partial X} & \frac{\partial u}{\partial Y} \\ \frac{\partial v}{\partial X} & 1 + \frac{\partial v}{\partial Y} \end{bmatrix}$$

where u and v stand for the velocities of the material particle. The time history of the surface average local deformation gradient y1 component over the microcapsule shell can be recorded within the Comsol software. Due to symmetry, the y1 component is the inverse of the x2 component in our case, thus only the y1 component is used to reflect the deformation response of the microcapsule. Among the three cases with different microcapsule thicknesses in this work, the δ*=0.4 configuration seems to be the most appropriate case since it is neither too sensitive nor insensitive to external loads as the δ*=0.2 case and the δ*=0.6 case. Therefore the microcapsule with $\delta^* = 0.4$ was chosen as a representative case for this study, under flow velocities from 0.05 m/s to 0.2 m/s at an incremental step of 0.05 m/s (same as previous sections of this work). The same reasoning also applies to the following investigation regarding the effects of different Young's Modulus. The results are shown in Figure 4B. For one microcapsule, its deformation trend is heavily affected by the flow velocity, that is, with a higher velocity, the microcapsule tends

to deform more dramatically. It is worth noting that our current settings resulted in some inconsistent convergence performances for different cases, as shown in Figure 4B in the manuscript, especially for the 0.15 m/s case, the calculation stopped due to convergence issues, and we were not able to produce the final deformation level for this case. With a clear trend being shown from produced data, the current results are considered sufficient to illustrate the deformation behavior of such microcapsules for this work.

Moreover, a negative tendency can be observed at the beginning for higher velocity cases. Because of the modeled microcapsule's elastic nature, this tendency can be considered as an elastic energy storage-relax process, which corresponds to the previously discussed microcapsule acceleration process in the moving fluid from its initial position. It can also be observed that this process is severer under higher flow velocities, yet for small flow velocities, such a phenomenon is less obvious until completely absent. To further investigate this elastic energy storage-relax process, with the tools provided within Comsol, we integrated the elastic strain energy over the microcapsule shell to produce total strain energy stored in the capsule shell due to deformation for every time step. In each configuration we investigated in this work, a rapid energy storage process in the microcapsule shell can be observed at the beginning and followed by a slower energy relaxing process can be observed. Such energy storage-relax process with the microcapsule with $\delta^* = 0.4$ under various flow velocities are shown in Figure 4C. It can be observed that higher flow velocity induced storage-relax process tend to be more rapid. Also, it can be observed from Figure 4D that due to the shell being thicker, when under similar circumstances, although stress-wise less concentrated (as shown in Figure 4A), the microcapsules with thicker shells (larger δ^*) tend to exhibit better capabilities to store strain energy.

Microcapsules with different Young's Modulus were also investigated. The same δ^* = 0.4 microcapsules were used, under a flow velocity of 0.15 m/s. Four different Young's Modulus was adopted: 750 kPa (baseline), 600 kPa, 450 kPa, and 300 kPa. The results of the microcapsules' deformation responses are shown in the left subfigure in Figure 5 with each case's von Mises stress distribution over the microcapsule shell at 0.05 s shown in the right subfigure in Figure 5.

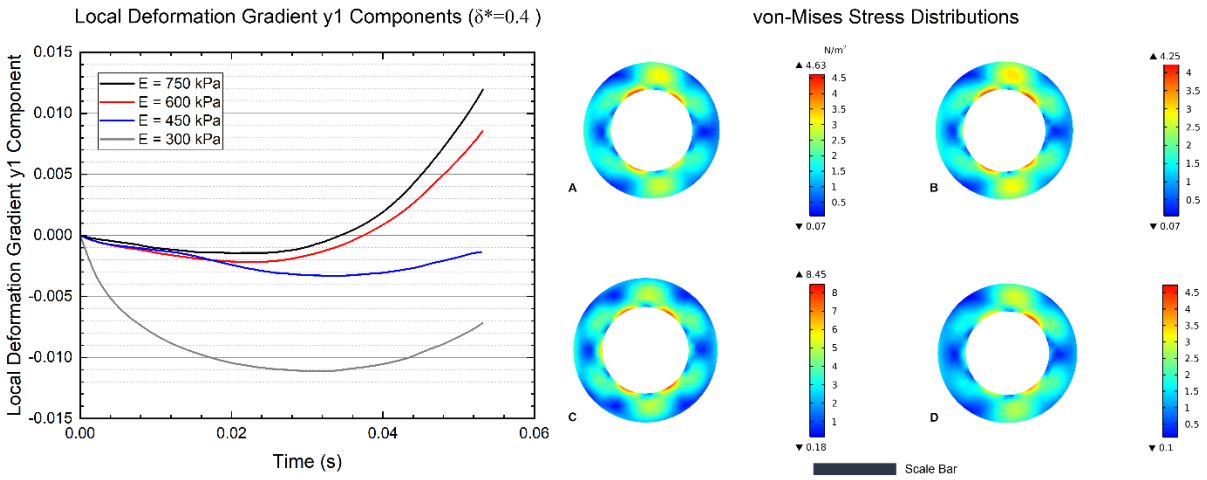

Figure 5 Left: The local deformation gradient y1 component of the microcapsule of δ*=0.4 at 0.15 m/s with different Young's Modulus; Right: Images of von Mises stress distribution over microcapsule shells of different Young's Modulus at 0.05 s, from subplot A to D corresponds to E=750 kPa, 600 kPa, 450 kPa, and 300 kPa. Microcapsule shell thickness δ*=0.4, with an inflow velocity of 0.15 m/s. The scale bar represents 0.2 mm

It can be observed that, with a smaller Young's Modulus, the microcapsule's ability to relax from the initial energy charge process decreases. For stiffer microcapsules, that is, with a higher shell Young's Modulus, it can be inferred that the flow shear stress from the fully developed laminar pipe flow is most responsible for the deformation of the capsule. Yet for softer ones, at initial time

steps, the force imposed on the microcapsule by the moving fluid plays a more significant role in the microcapsule's deformation. Also, as one could imagine, the stiffer microcapsules are more capable of relaxing from the initial energy storage, which leads to a negative deformation in terms of the plotted local deformation gradient y1 component. From the right subfigure in Figure 5 it can be seen that the distribution of von-Mises Stress is not much influenced by the change of Young's Modulus.

4. Conclusions

A 2D numerical model was developed to investigate the fluid-structure interactions between fully developed pipe flow and core-shell structured microcapsules, various flow velocities, and microcapsule shell thicknesses were considered. The developed model was validated with theoretical calculations and a monitor framework was proposed to estimate whether the microcapsule is being stably carried along by the moving fluid. Upon analyzing the von Mises stress distribution over the microcapsule shell, and investigating the surface average von Mises stress of each configuration as well as looking into the microcapsule's shell surface average local deformation gradient y1 component, several conclusions can be drawn:

- For all proposed configurations, symmetrical distribution of von-Mises Stress over the shell can be observed along the flow direction
- A 6^{th} order rotational symmetric distribution of von Mises stress over the microcapsule shell can also be observed on microcapsules with thinner shells (namely $\delta^* = 0.2$ and $\delta^* = 0.4$), especially at higher flow velocities
- When being carried along in a fully developed pipe flow, the microcapsule with a thinner shell tends to accumulate stress at a higher rate compared to that of a thicker shell

- Generally, a higher flow velocity and a thinner microcapsule shell would lead to higher overall stress imposed on the capsule shell
- A microcapsule's deformation is heavily affected by the flow velocity. The higher the flow velocity, the more dramatically the microcapsule tends to deform
- An elastic energy storage-relax process can be observed during the microcapsule's acceleration process
- The mechanical properties of microcapsule shells such as Young's Modulus can also affect its deformation in a significant way, even with similar distributions of von-Mises stress over the shells of the microcapsules.

Conflicts of interest

The authors declare no conflict of interest.

Data Availability Statement

The data that support the findings of this study are available from the corresponding author upon reasonable request.

Acknowledgements

This work was financially supported by Zhejiang Provincial Natural Science Foundation of China under grant No. LY19E060001 and LQ19F050003, Ningbo Science and Technology Bureau under Service Industry Science & Technology Programme with project code 2019F1030. The Zhejiang Provincial Department of Science and Technology is also acknowledged for this research under its Provincial Key Laboratory Programme (2020E10018).

References

[1] Wang, J., Li, Y., Wang, X., Wang, J., Tian, H., Zhao, P., Tian, Y., Gu, Y., Wang, L., Wang, C., Micromachines 2017, 8, 22.

[2] Wang, B., Prinsen, P., Wang, H., Bai, Z., Wang, H., Luque, R., Xuan, J., Chem. Soc. Rev. 2017, 46, 855–914.

[3] Bouchemal, K., Briançon, S., Perrier, E., Fessi, H., Bonnet, I., Zydowicz, N., Int. J. Pharm. 2004, 269, 89–100.

[4] Dowding, P. J., Atkin, R., Vincent, B., Bouillot, P., Langmuir 2004, 20, 11374–11379.

[5] Chen, H., Zhao, Y., Song, Y., Jiang, L., J. Am. Chem. Soc. 2008, 130, 7800–7801.

[6] Joanicot, M., Ajdari, A., Science 2005, 309, 887–888.

[7] Zhu, P., Wang, L., Lab Chip 2017, 17, 34–75.

[8] Datta, S. S., Abbaspourrad, A., Amstad, E., Fan, J., Kim, S., Romanowsky, M., Shum, H. C., Sun, B., Utada, A. S., Windbergs, M., Adv. Mater. 2014, 26, 2205–2218.

[9] Ren, Y., Liu, Z., Shum, H. C., Lab Chip 2015, 15, 121–134.

[10] Ren, Y., Seng Koh, K., Kai Chin, J., Wang, J., Wen, C., Yan, Y., J. Heat Transfer 2018, 140.

[11] Ren, Y., Koh, K. S., Yew, M., Chin, J. K., Chan, Y., Yan, Y., Micromachines 2018, 9, 57.

[12] Lee, S. S., Kim, B., Kim, S. K., Won, J. C., Kim, Y. H., Kim, S., Adv. Mater. 2015, 27, 627–633.

[13] Nisisako, T., Hatsuzawa, T., Sensors Actuators B Chem. 2016, 223, 209–216.

[14] Zhang, L., Cai, L., Lienemann, P. S., Rossow, T., Polenz, I., Vallmajo‐Martin, Q., Ehrbar, M., Na, H., Mooney, D. J., Weitz, D. A., Angew. Chemie 2016, 128, 13668–13672.

[15] Jeong, W. J., Kim, J. Y., Choo, J., Lee, E. K., Han, C. S., Beebe, D. J., Seong, G. H., Lee, S. H., Langmuir 2005, 21, 3738–3741.

[16] Shang, L., Shangguan, F., Cheng, Y., Lu, J., Xie, Z., Zhao, Y., Gu, Z., Nanoscale 2013, 5, 9553–9557.

[17] Shah, R. K., Kim, J., Weitz, D. A., Adv. Mater. 2009, 21, 1949–1953.

[18] Tan, W., Takeuchi, S., Adv. Mater. 2007, 19, 2696–2701.

[19] Lee, D., Weitz, D. A., Adv. Mater. 2008, 20, 3498–3503.

[20] Park, J. Il, Nie, Z., Kumachev, A., Abdelrahman, A. I., Binks, B. P., Stone, H. A., Kumacheva, E., Angew. Chemie 2009, 121, 5404–5408.

[21] Shum, H. C., Lee, D., Yoon, I., Kodger, T., Weitz, D. A., Langmuir 2008, 24, 7651–7653.

[22] Lim, C. N., Koh, K. S., Ren, Y., Chin, J. K., Shi, Y., Yan, Y., Micromachines 2017, 8, 49.

[23] Ren, Y., Leung, W. W. F., Micromachines 2016, 7, 17.

[24] Lian, Z., Wei, C., Gao, B., Yang, X., Chan, Y., Wang, J., Chen, G. Z., Koh, K. S., Shi, Y., Yan, Y., RSC Adv. 2020, 10, 9210–9225.

[25] Yew, M., Ren, Y., Koh, K. S., Sun, C., Snape, C., Glob. Challenges 2019, 3, 1800060.

[26] Ren, Y., Chan, Y., Yang, C., Wang, J., J. Therm. Sci. Eng. Appl. 2020, 12.

[27] Lian, Z., Chan, Y., Luo, Y., Yang, X., Koh, K. S., Wang, J., Chen, G. Z., Ren, Y., He, J., Electrophoresis 2020, 41, 891–901.

[28] Lian, Z., Ren, Y., He, J., Chen, G. Z., Koh, K. S., Microfluid. Nanofluidics 2018, 22, 1–13.

[29] Zhao, C.-X., Adv. Drug Deliv. Rev. 2013, 65, 1420–1446.

[30] Abbaspourrad, A., Datta, S. S., Weitz, D. A., Langmuir 2013, 29, 12697–12702.

[31] Kim, S.-H., Kim, J. W., Cho, J.-C., Weitz, D. A., Lab Chip 2011, 11, 3162–3166.

[32] Sun, B. J., Shum, H. C., Holtze, C., Weitz, D. A., ACS Appl. Mater. Interfaces 2010, 2, 3411–3416.

[33] Abbaspourrad, A., Carroll, N. J., Kim, S.-H., Weitz, D. A., J. Am. Chem. Soc. 2013, 135, 7744–7750.

[34] Shang, L., Cheng, Y., Zhao, Y., Chem. Rev. 2017, 117, 7964–8040.

[35] Walter, J., Salsac, A., Barthès-Biesel, D., Le Tallec, P., Int. J. Numer. Methods Eng. 2010, 83, 829–850.

[36] Walter, J., Salsac, A.-V., Barthes-Biesel, D., J. Fluid Mech. 2011, 676, 318–347.

[37] Foessel, E., Walter, J., Salsac, A.-V., Barthès-Biesel, D., J. Fluid Mech. 2011, 672, 477–486.

[38] Hu, X.-Q., Salsac, A.-V., Barthès-Biesel, D., J. Fluid Mech. 2012, 705, 176–194.

[39] Dupont, C., Salsac, A.-V., Barthes-Biesel, D., Vidrascu, M., Le Tallec, P., Phys. Fluids 2015, 27, 51902.

[40] Zhu, L., Brandt, L., J. Fluid Mech. 2015, 770, 374–397.

[41] Müller, K., Fedosov, D. A., Gompper, G., Sci. Rep. 2014, 4, 1–8.

[42] Caballero, D., Blackburn, S. M., De Pablo, M., Samitier, J., Albertazzi, L., Lab Chip 2017, 17, 3760–3771.

[43] Chakraborty, D., Prakash, J. R., Friend, J., Yeo, L., Phys. Fluids 2012, 24, 102002.

[44] Incropera, F. P., DeWitt, D. P., Bergman, T. L., Lavine, A. S., Fundamentals of Heat and Mass Transfer. Wiley New York 1996.

[45] Mercadé-Prieto, R., Allen, R., Zhang, Z., York, D., Preece, J. A., Goodwin, T. E., AIChE J. 2012, 58, 2674–2681.

[46] Biswas, B. N., Chatterjee, S., Mukherjee, S. P., Pal, S., Electron. J. Math. Anal. Appl. 2013, 1, 2090–2792.

[47] White, F. M., New York 1994.

[48] Ozturk, Y., 1972.

[49] Do Nascimento, D. F., Avendaño, J. A., Mehl, A., Moura, M. J. B., Carvalho, M. S., Duncanson, W. J., Sci. Rep. 2017, 7, 1–7.